

# Lawrence Berkeley National Laboratory

## Recent Work

### Title

Azimuthal anisotropy of photon and charged particle emission in  $208\text{Pb} + 208\text{Pb}$  collisions at  $158 \text{ A} \sqrt{s} \text{ GeV/c}$

### Permalink

<https://escholarship.org/uc/item/9tx6469n>

### Journal

The European Physical Journal C, 41(3)

### ISSN

1434-6044

### Authors

Aggarwal, MM  
Ahammed, Z  
Angelis, ALS  
et al.

### Publication Date

2005-06-01

### DOI

10.1140/epjc/s2005-02249-2

Peer reviewed

# Azimuthal anisotropy of photon and charged particle emission in $^{208}\text{Pb} + ^{208}\text{Pb}$ collisions at $158 \cdot A \text{ GeV}/c$

The WA98 Collaboration

M.M. Aggarwal<sup>4</sup>, Z. Ahammed<sup>2</sup>, A.L.S. Angelis<sup>7,†</sup>, V. Antonenko<sup>13</sup>, V. Arefiev<sup>6</sup>, V. Astakhov<sup>6</sup>, V. Avdeitchikov<sup>6</sup>, T.C. Awes<sup>16</sup>, P.V.K.S. Baba<sup>10</sup>, S.K. Badyal<sup>10</sup>, S. Bathe<sup>14</sup>, B. Batiounia<sup>6</sup>, T. Bernier<sup>15</sup>, V.S. Bhatia<sup>4</sup>, C. Blume<sup>14</sup>, D. Bucher<sup>14</sup>, H. Büsching<sup>14</sup>, L. Carlén<sup>12</sup>, S. Chattopadhyay<sup>2</sup>, M.P. Decowski<sup>3</sup>, H. Delagrange<sup>15</sup>, P. Donni<sup>7</sup>, M.R. Dutta Majumdar<sup>2</sup>, A.K. Dubey<sup>1</sup>, K. El Chenawi<sup>12</sup>, K. Enosawa<sup>18</sup>, S. Fokin<sup>13</sup>, V. Frolov<sup>6</sup>, M.S. Ganti<sup>2</sup>, S. Garpman<sup>12,†</sup>, O. Gavrishchuk<sup>6</sup>, F.J.M. Geurts<sup>19</sup>, T.K. Ghosh<sup>8</sup>, R. Glasow<sup>14</sup>, R. Gupta<sup>10</sup>, B. Guskov<sup>6</sup>, H.Å. Gustafsson<sup>12</sup>, H.H. Gutbrod<sup>5</sup>, I. Hrivnacova<sup>17</sup>, M. Ippolitov<sup>13</sup>, H. Kalechovsky<sup>7</sup>, R. Kamermans<sup>19</sup>, K. Karadjev<sup>13</sup>, K. Karpio<sup>20</sup>, B.W. Kolb<sup>5</sup>, I. Kosarev<sup>6</sup>, I. Koutcheryaev<sup>13</sup>, A. Kugler<sup>17</sup>, P. Kulinich<sup>3</sup>, M. Kurata<sup>18</sup>, A. Lebedev<sup>13</sup>, H. Löhner<sup>8</sup>, L. Luquin<sup>15</sup>, D.P. Mahapatra<sup>1</sup>, V. Manko<sup>13</sup>, M. Martin<sup>7</sup>, G. Martínez<sup>15</sup>, A. Maximov<sup>6</sup>, Y. Miake<sup>18</sup>, G.C. Mishra<sup>1</sup>, B. Mohanty<sup>2</sup>, M.-J. Mora<sup>15</sup>, D. Morrison<sup>11</sup>, T. Moukhanova<sup>13</sup>, D.S. Mukhopadhyay<sup>2</sup>, H. Naef<sup>7</sup>, B.K. Nandi<sup>2</sup>, S.K. Nayak<sup>10</sup>, T.K. Nayak<sup>2</sup>, A. Nianine<sup>13</sup>, V. Nikitine<sup>6</sup>, S. Nikolaev<sup>13</sup>, P. Nilsson<sup>12</sup>, S. Nishimura<sup>18</sup>, P. Nomokonov<sup>6</sup>, J. Nystrand<sup>12</sup>, A. Oskarsson<sup>12</sup>, I. Otterlund<sup>12</sup>, T. Peitzmann<sup>19</sup>, D. Peressounko<sup>13</sup>, V. Petrache<sup>17</sup>, S.C. Phatak<sup>1</sup>, W. Pinganaud<sup>15</sup>, F. Plasil<sup>16</sup>, M.L. Purschke<sup>5</sup>, J. Rak<sup>17</sup>, R. Raniwala<sup>9,a</sup>, S. Raniwala<sup>9</sup>, N.K. Rao<sup>10</sup>, F. Retiere<sup>15</sup>, K. Reygers<sup>14</sup>, G. Roland<sup>3</sup>, L. Rosset<sup>7</sup>, I. Roufanov<sup>6</sup>, C. Roy<sup>15</sup>, J.M. Rubio<sup>7</sup>, S.S. Sambyal<sup>10</sup>, R. Santo<sup>14</sup>, S. Sato<sup>18</sup>, H. Schlagheck<sup>14</sup>, H.-R. Schmidt<sup>5</sup>, Y. Schutz<sup>15</sup>, G. Shabratova<sup>6</sup>, T.H. Shah<sup>10</sup>, A. Sharma<sup>10</sup>, I. Sibiriak<sup>13</sup>, T. Siemiarczuk<sup>20</sup>, D. Silvermyr<sup>12</sup>, B.C. Sinha<sup>2</sup>, N. Slavine<sup>6</sup>, K. Söderström<sup>12</sup>, G. Sood<sup>4</sup>, S.P. Sørensen<sup>11</sup>, P. Stankus<sup>16</sup>, G. Stefanek<sup>20</sup>, P. Steinberg<sup>3</sup>, E. Stenlund<sup>12</sup>, M. Sumera<sup>17</sup>, T. Svensson<sup>12</sup>, A. Tsvetkov<sup>13</sup>, L. Tykarski<sup>20</sup>, E.C. v.d. Pijll<sup>19</sup>, N. v. Eijndhoven<sup>19</sup>, G.J. v. Nieuwenhuizen<sup>3</sup>, A. Vinogradov<sup>13</sup>, Y.P. Viyogi<sup>2</sup>, A. Vodopianov<sup>6</sup>, S. Vörös<sup>7</sup>, B. Wysłouch<sup>3</sup>, G.R. Young<sup>16</sup>

<sup>1</sup> Institute of Physics, 751-005 Bhubaneswar, India

<sup>2</sup> Variable Energy Cyclotron Centre, Calcutta 700 064, India

<sup>3</sup> MIT Cambridge, MA 02139, USA

<sup>4</sup> University of Panjab, Chandigarh 160014, India

<sup>5</sup> Gesellschaft für Schwerionenforschung (GSI), 64220 Darmstadt, Germany

<sup>6</sup> Joint Institute for Nuclear Research, 141980 Dubna, Russia

<sup>7</sup> University of Geneva, 1211 Geneva 4, Switzerland

<sup>8</sup> KVI, University of Groningen, 9747 AA Groningen, The Netherlands

<sup>9</sup> University of Rajasthan, Jaipur 302004, Rajasthan, India

<sup>10</sup> University of Jammu, Jammu 180001, India

<sup>11</sup> University of Tennessee, Knoxville, Tennessee 37966, USA

<sup>12</sup> Lund University, 221 00 Lund, Sweden

<sup>13</sup> RRC “Kurchatov Institute”, 123182 Moscow, Russia

<sup>14</sup> University of Münster, 48149 Münster, Germany

<sup>15</sup> SUBATECH, Ecole des Mines, Nantes, France

<sup>16</sup> Oak Ridge National Laboratory, Oak Ridge, Tennessee 37831-6372, USA

<sup>17</sup> Nuclear Physics Institute, 250 68 Rez, Czech Republic

<sup>18</sup> University of Tsukuba, Ibaraki 305, Japan

<sup>19</sup> Universiteit Utrecht/NIKHEF, 3508 TA Utrecht, The Netherlands

<sup>20</sup> Institute for Nuclear Studies, 00-681 Warsaw, Poland

<sup>†</sup> Deceased

Received: 22 May 2004 / Revised version: 14 April 2005 /

Published online: 4 May 2005 – © Springer-Verlag / Società Italiana di Fisica 2005

**Abstract.** The azimuthal distributions of photons and charged particles with respect to the event plane are investigated as a function of centrality in  $^{208}\text{Pb} + ^{208}\text{Pb}$  collisions at  $158 \cdot A \text{ GeV}/c$  in the WA98 experiment at the CERN SPS. The anisotropy of the azimuthal distributions is characterized using a Fourier analysis. For both the photon and charged particle distributions the first two Fourier coefficients are observed to decrease with increasing centrality. The observed anisotropies of the photon distributions compare well with the expectations from the charged particle measurements for all centralities.

**PACS.** 25.75.Dw

## 1 Introduction

Non-isotropic emission of particles with respect to the reaction plane, as first observed at the Bevalac [1], provides evidence for collective flow in high energy heavy ion collisions. Flow, or anisotropic particle emission, has been observed for a large variety of interacting systems from incident energies of a few A GeV/c at the Bevalac (SIS) and AGS to much greater energies at the SPS and RHIC [2–13].

Anisotropic flow manifests itself as asymmetries in the azimuthal distribution of particles and can be reproduced in theoretical models with different underlying assumptions. One scenario is incorporated in transport models where the particles have a mean free path comparable to the system size [14–16]. The models can describe the observed flow up to AGS energies. The other scenario applies when the mean free path is much smaller than the system size which allows the description of the equilibrated system in terms of macroscopic quantities [17, 18]. Hydrodynamic models are able to describe the qualitative features of the observed flow [19] for  $p_T$  below about 3 GeV/c.

The initial asymmetry in the overlap zone of the colliding nuclei translates into unequal pressure gradients in different directions that leads to an elliptic final state momentum distribution of the particles [17], causing an elliptic pattern of flow. The elliptic flow is therefore expected to be sensitive to the system evolution at the time of maximum compression [20] and is shown to be sensitive to the equation of state of the compressed nuclear matter. The variation of asymmetry with centrality enables to relate the observed flow to the geometry of the overlap region [21, 16]. One would then expect a scaling of the data from AGS to SPS and RHIC provided the physics of elliptic flow remains the same [22]. In the case that there is a phase transition from hadronic matter to a quark gluon plasma, it is expected that the reflection of this transition in the equation of state of the dense nuclear matter would result in changes in the pressure gradients which would then be reflected in changes in the particle flow pattern.

The first evidence of azimuthal anisotropy at SPS energies was observed in the distribution of photons from S+Au collisions at 200 A GeV measured in the preshower photon multiplicity detector of the WA93 experiment at CERN [8]. Since almost 90% of photons produced in ultra-relativistic nuclear collisions originate from the decay of  $\pi^0$ 's, the anisotropy of the observed photon distributions should reflect the anisotropy of the  $\pi^0$  production followed by the effects of decay of the  $\pi^0$ 's. Methods have been proposed to estimate the anisotropy of the neutral pion emission by measuring the anisotropy of photons [23]. The decay introduces non-flow correlations between the photon pairs due to four-momentum conservation and may dilute the correlations between the  $\pi^0$ 's and the event plane. Determination of the effect of decay enables the deduction of the anisotropy of the neutral pions. The photon anisotropy measurement thus complements the study of the anisotropy of charged particle distributions.

In the present work we report results from the WA98 experiment on the centrality dependence of the anisotropy coefficients extracted from measurement of the azimuthal distributions with respect to the event plane of photons and charged particles in the same pseudorapidity interval. Preliminary results on the anisotropy of photon emission in Pb+Pb collisions have been reported earlier [24, 25]. The paper is organized in the following manner: Sect. 2 describes the experimental setup and data selection. The analysis technique is discussed in Sect. 3. The results on the centrality dependence of the azimuthal anisotropy of charged particles and photons are discussed in Sect. 4 and Sect. 5 summarises our investigations.

## 2 WA98 experiment and data selection

The WA98 experiment at CERN [26] placed emphasis on simultaneous detection of hadrons and photons. The experimental setup consisted of large acceptance hadron and photon spectrometers, detectors for photon and charged particle multiplicity measurements, and calorimeters for transverse and forward energy measurements. The experiment recorded data with 158 A GeV Pb beams from the CERN SPS in 1994, 1995, and 1996. The results presented here are from a portion of the Pb run in 1996 during which the magnet (GOLIATH) was turned off. The analysis presented here used data recorded with the photon multiplicity detector (PMD) and the silicon pad multiplicity detector (SPMD). The data from the mid-rapidity calorimeter (MIRAC) was used to characterize events on the basis of centrality of the collision.

The circular Silicon Pad Multiplicity Detector (SPMD), used for measurement of the charged particle multiplicity, was located 32.8 cm from the target. It had full azimuthal coverage in the region  $2.35 \leq \eta \leq 3.75$  (beam rapidity  $y_{\text{beam}} = 5.81$ ). The detector had four overlapping quadrants, each fabricated from a single 300  $\mu\text{m}$  thick silicon wafer. The active area of each quadrant was divided into 1012 pads forming 46 azimuthal wedges and 22 radial bins with pad size increasing with radius to provide a uniform pseudo-rapidity coverage. The intrinsic efficiency of the detector was better than 99%. During the data taking, 95% of the pads worked properly. The SPMD was nearly transparent to high energy photons since only about 0.2% are expected to interact in the silicon. Multiple hits of charged particles on a single pad were treated as a single hit for the present analysis, and are counted as  $N_{\text{hits}}$ . The detector is sensitive to all charged particles. The energy cutoff appears as a low noise threshold. Details of the characteristics of the SPMD can be found in [27, 28].

The photon multiplicity was measured using the preshower photon multiplicity detector (PMD) located at a distance of 21.5 meters from the target. The detector consisted of 3 radiation length ( $X_0$ ) thick lead converter plates placed in front of an array of square scintillator pads of four different sizes that varied from 15 mm  $\times$  15 mm to 25 mm  $\times$  25 mm, placed in 28 box modules. Each box module had a matrix of 38  $\times$  50 pads which were read

<sup>a</sup> e-mail: rashmi@mail.cern.ch

**Table 1.** Centrality selections used in the present analysis based on the measured total transverse energy. The corresponding fraction of the minimum bias cross section, number of participants, and the average photon and charged particle multiplicities measured in the pseudo-rapidity interval  $3.25 \leq \eta \leq 3.75$  are given for each centrality selection

$E_T$ (GeV)	% $\sigma_{MB}$	$N_{\text{part}}$	$\langle N_{\text{photon}} \rangle$	$\langle N_{\text{hits}} \rangle$
40.0–89.9	50–80	43.7	41.1	34.3
89.9–124.3	40–50	87.5	65.6	56.9
124.3–170.2	30–40	123.0	88.0	78.1
170.2–225.5	20–30	172.2	116.9	105.5
225.5–298.6	10–20	237.7	163.1	150.5
298.6–347.6	5–10	300.4	190.1	177.1
>347.6	0–5	353.4	222.9	210.3

out using one image intensifier + CCD camera. Details of the design and characteristics of the PMD may be found in [29, 30].

The clusters of hit pads with a signal above a hadron rejection threshold were identified as photon-like. The present analysis has been performed with the photon-like clusters, which are referred to as photons for brevity. Detailed simulations showed that the photon counting efficiencies for the central to peripheral cases varied from 68% to 73%. The purity of the photon sample in the two cases varied from 65% to 54%. Most of the contaminants of the photon sample are charged particles which deposit enough energy to fall above the hadron rejection threshold. The hadron rejection threshold is taken as three times the energy deposited by a minimum ionizing particle. For photons this leads to a low  $p_T$  threshold of 30 MeV/c.

The transverse energy was measured with the MIRAC calorimeter [31] located at 24.7 meters downstream from the target. The MIRAC was used to measure the total transverse energy by measurement of both the transverse electromagnetic ( $E_T^{\text{em}}$ ) and hadronic ( $E_T^{\text{had}}$ ) energies in the pseudorapidity interval  $3.5 \leq \eta \leq 5.5$ . The measured total transverse energy,  $E_T$ , provides a measure of the centrality of the reaction. Events with large  $E_T$  correspond to very central reactions with small impact parameter, and vice versa.

The minimum bias  $E_T$  distribution has been divided into different fractions of the minimum bias cross section corresponding to different centrality bins [30]. The most central selection corresponds to that 5% of the minimum bias cross section  $\sigma_{MB}$  with largest measured  $E_T$ . A total of about 0.25 Million events have been analysed. The minimum number of events in any centrality selection is 15K and the maximum is 70K. Table 1 shows the percentage cross section and the corresponding number of participants for each centrality bin. The results presented here use only the data for the pseudorapidity region of common coverage of the PMD and SPMD ( $3.25 \leq \eta \leq 3.75$ ) where both detectors have full azimuthal coverage. The average measured photon and charged particle multiplici-

ties for this region of acceptance are also quoted for each centrality in Table 1.

### 3 Analysis

The anisotropy of the azimuthal distribution of particle emission with respect to the reaction plane (or event plane) is characterized by the coefficients of the Fourier expansion of the azimuthal distribution [32]. The first and the second coefficients are measures of the directed and elliptic flow when the expansion is made about the reaction plane, the plane defined by the beam direction and the impact parameter. This may be written as

$$\frac{2\pi dN}{d(\phi - \psi_R)} = 1 + 2v_1 \cos(\phi - \psi_R) + 2v_2 \cos 2(\phi - \psi_R) \quad (1)$$

where  $\phi$  is the azimuthal angle of the measured particle and  $\psi_R$  denotes the azimuthal orientation of the reaction plane. The reaction plane can be most accurately determined in an experiment that measures the (transverse) momenta of the target or projectile fragments. Both  $v_1$  and  $v_2$  can take positive or negative values. By convention, positive (negative) values of  $v_1$  in (1) denote flow (anti-flow) in the direction of the deflected projectile fragment, and positive (negative) values of  $v_2$  indicate in-plane (out-of-plane) flow.

Though the most accurate determination of the reaction plane requires the measurement of target (or projectile) fragments, most experiments *assume* that the measurement of any particle type, in any kinematic window enables a determination of the reaction plane. We wish to distinguish between the plane determined by projectile or target fragments and the plane determined by any other particle type, and throughout this article refer to the latter as the *event plane*. Obtaining the values of coefficients after projecting azimuthal angles on the event plane determined from the same set (after removing auto correlations) maximises the values of anisotropy coefficients, and may include non-flow correlations. The values obtained are necessarily positive, and have been shown as such in the present work. The coefficients determined by projecting on an event plane from any other set of particles are expected to be smaller, and can also have negative values. The difference in the values determined using different sets of event planes have been included in systematic error by various experiments [10, 11, 13].

#### 3.1 Method

In the present analysis, the azimuthal distributions of particles for any particle species in any pseudorapidity window is expanded as a Fourier series where the coefficients of expansion determine the shape of the event. Retaining terms up to second order coefficient in the expansion, the shape can be characterized by an ellipse for small values of

the coefficients. The direction of the centroid and the major axis of the ellipse are determined from the azimuthal distributions of the particles. These directions, along with the beam direction, define the first order and the second order event plane respectively, and are obtained as [32]

$$\psi'_m = \frac{1}{m} \left( \tan^{-1} \frac{\sum w_i \sin m\phi_i}{\sum w_i \cos m\phi_i} \right) \quad (2)$$

where  $m = 1$  or  $2$  for the first and the second order, respectively. The  $\phi_i$  are the azimuthal angles of the emitted particles with respect to a fixed laboratory direction and the  $w_i$  are the weight factors. For the azimuthal distribution of the particle yield, as in (1), the weight factors are set equal to one. In reality, due to finite particle multiplicities  $\psi'_1$  and  $\psi'_2$  fluctuate about the *actual* event planes that represent the direction of the centroid and the direction of the major axis of the elliptic shape. To the extent that initial state nuclear densities are spherically symmetric and the density fluctuations are negligible, the initial nucleon density in the overlap region is symmetric about the impact parameter or reaction plane and so it is expected that the two event plane angles are either the same or perpendicular to the reaction plane.

The anisotropy, or Fourier coefficients of order  $n$ , can be determined from the azimuthal distribution of the particles with respect to the event plane angle of order  $m$ , provided  $n$  is an integral multiple of  $m$ , by fitting to the following equation [32]

$$\frac{dN}{d(\phi - \psi'_m)} \propto 1 + \sum_{n=1}^{\infty} 2v'_{nm} \cos nm(\phi - \psi'_m) \quad (3)$$

$v'_{nm}$  is a measure of the offset of the centroid of the distribution when  $n \cdot m = 1$  and is a measure of the difference between the major and the minor axes of the ellipse when  $n \cdot m = 2$ . The actual coefficients are obtained from the observed coefficients  $v'_{nm}$  as described later.

Since the event planes do not depend on the geometrical setup of the experiment, the distribution of the event plane angles determined for a large number of events is expected to be uniformly distributed in laboratory angle. Any non-uniformity in the acceptance of the detectors over the full azimuth will be reflected in a non-uniform distribution of event plane angles. Any non-uniformity that is identifiable within a large subset of events can be corrected for by appropriate correction methods. The method employed in the present work is summarized in the following.

### 3.2 Detector acceptance correction

The corrected event plane angle is obtained by shifting the observed event plane angles  $\psi'_m$  by  $\Delta\psi'_m$  [32] where the latter is written as

$$\Delta\psi'_m = \sum_{n=1}^N \frac{2}{nm} (-\langle \sin(nm \psi'_m) \rangle \cos(nm \psi'_m) + \langle \cos(nm \psi'_m) \rangle \sin(nm \psi'_m)) \quad (4)$$

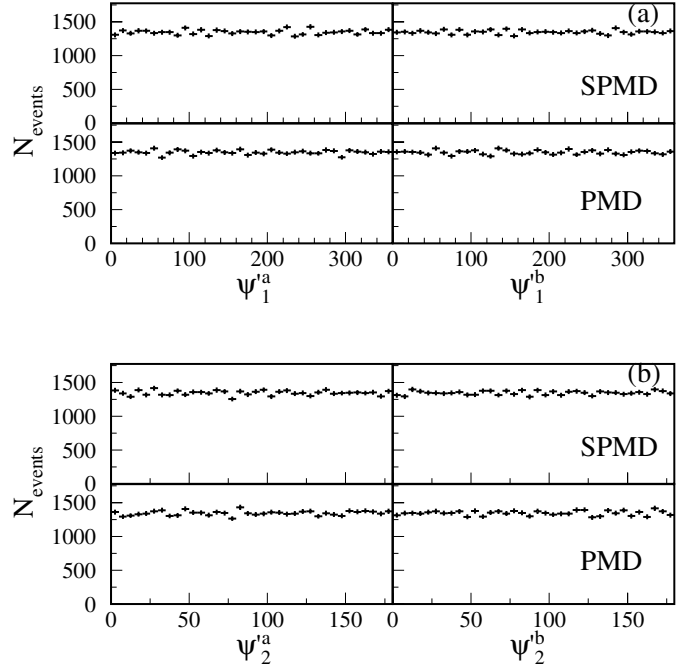


**Fig. 1.** Acceptance corrected distributions of **a** the first order event plane angle,  $\psi'_1$ , of the two subevents for the charged particles hits in the SPMD and the photons in the PMD in the region  $3.25 \leq \eta \leq 3.75$  for the centrality class defined by  $225.5 \leq E_T \leq 298.6$ . **b** The same for second order event plane angle,  $\psi'_2$

where  $N = 4/m$  is sufficient to flatten the raw  $\psi$  distribution. The angular brackets denote an average over all events and are obtained from the raw distribution of the  $m^{\text{th}}$  order event plane distribution.

The distribution of the first and the second order event plane angles, corrected for acceptance, is shown in Fig. 1 for the charged particle hits in the SPMD and the photon hits in the PMD.

### 3.3 Event plane resolution correction

The average deviation of the estimated event plane from the true event plane due to multiplicity fluctuations can be determined experimentally and is termed as the resolution correction factor (RCF). Experimentally, RCF is obtained using the subevent method described in [32]. The particles in each event are sorted in ascending order of pseudorapidity. Each event is divided into two equal multiplicity subevents separated by a pseudorapidity interval. The two subevents are separated by one pad for the SPMD and by  $\Delta\eta = 0.05$  for the PMD. The actual location of the pad in SPMD and the  $\Delta\eta$  interval in PMD is allowed to vary in the region 3.25 to 3.75 to ensure equal multiplicity for the two subevents. The event plane angle  $\psi'_m$  is determined for each subevent.<sup>1</sup>

<sup>1</sup> The distribution of the corrected event plane angles for these subevents is observed to be flat, for both orders, for photons and for charged particles.

This enables determination of a parameter  $\chi_m$  directly from the experimental data using the fraction of events where the correlation of the planes of the subevents is greater than  $\pi/2$  [32,33]:

$$\frac{N_{\text{events}}(m|\psi_m'^a - \psi_m'^b| > \pi/2)}{N_{\text{total}}} = \frac{e^{-\frac{\chi_m^2}{4}}}{2} \quad (5)$$

where  $N_{\text{total}}$  denotes the total number of events,  $\psi_m'^a$ ,  $\psi_m'^b$  are the observed event plane angles of the two subevents (labeled  $a$  and  $b$ ) and the numerator on the left denotes the number of events having the angle between subevents greater than  $\pi/2m$ . The parameter  $\chi_m$  so obtained is then used to determine  $\text{RCF}_{nm} = \langle \cos(nm(\psi_m' - \psi_m^{\text{true}})) \rangle$ , where  $\psi_m^{\text{true}}$  is the true direction of the event plane, and the average is over all events. The RCF can be determined from  $\chi_m$  by the following relation from reference [32].

$$\langle \cos(nm(\psi_m' - \psi_m^{\text{true}})) \rangle = \frac{\sqrt{\pi}}{2\sqrt{2}} \chi_m \exp(-\chi_m^2/4) \cdot \left[ I_{\frac{n-1}{2}}(\chi_m^2/4) + I_{\frac{n+1}{2}}(\chi_m^2/4) \right] \quad (6)$$

where  $I_\nu$  are the modified Bessel functions of order  $\nu$ .

The errors on the RCF values have been obtained by considering that the error on  $N_{\text{events}}$  is statistical. The new values of  $\chi_m$  are then calculated for values of  $N_{\text{events}} \pm \sqrt{N_{\text{events}}}$  and used in (6) to calculate new values of RCF. The change in the RCF values gives the statistical error on the RCF determination. In general, the errors determined in this way are asymmetric. Symmetric errors have been quoted using the larger of the two asymmetric errors.

### 3.4 Anisotropy coefficients

The anisotropy coefficients are obtained by filling up particle azimuthal distributions of one subevent with respect to the event plane of the other subevent where the subevent division is described in the previous section. The anisotropy coefficients have been determined by three methods which differ in detail and provide a consistency check. In this analysis the Fourier coefficients prior to event plane resolution correction  $v'_{nm}$  are extracted for the case with event plane order equal to the order of the extracted Fourier coefficient, i.e.  $v'_{nm} = v'_{nn}$  which we will denote by  $v'_n$ .

In the first method we determine  $v_n'^a = \langle \cos n(\phi^a - \psi_n'^a) \rangle$  and  $v_n'^b = \langle \cos n(\phi^b - \psi_n'^b) \rangle$  where  $\phi^a$  represent the azimuthal angles of particles in subevent  $a$  and  $\psi_n'^b$  is the event plane angle determined using particles in subevent  $b$ . The averages are computed over all particles over all events. In the absence of non-flow correlations,  $v_n$  can be determined using

$$v_n = \sqrt{\frac{v_n'^a \cdot v_n'^b}{\langle \cos n(\psi_n'^a - \psi_n'^b) \rangle}} \quad (7)$$

This determines the magnitude of the coefficients and is necessarily positive.

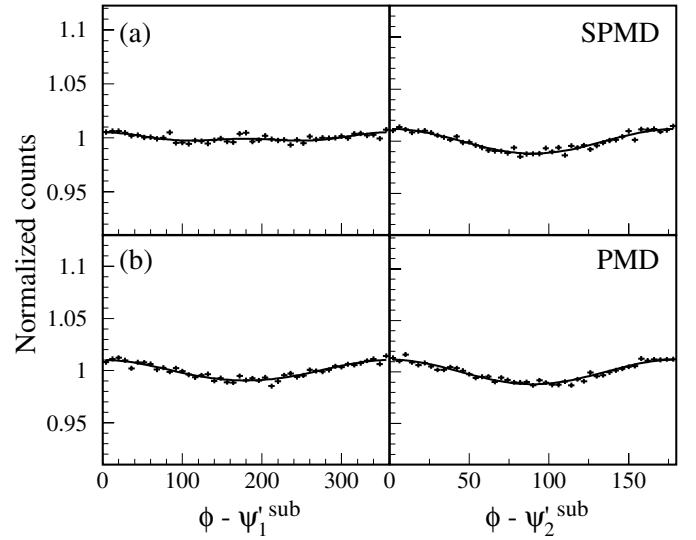


**Fig. 2.** Distributions of azimuthal angles with respect to the first and second order event plane for the centrality class defined by  $225.5 \leq E_T \leq 298.6$ . **a** for charged particle hits in the SPMD and **b** for photons in the PMD, both in the pseudorapidity region  $3.25 \leq \eta \leq 3.75$

The distributions with respect to the event plane are shown in Fig. 2 for both photon and charged particles, for both orders for the centrality selection corresponding to 10–20% of the cross section. In the second method the distributions have been fitted to (3) to determine  $v'_{11}$ . The corresponding distributions with respect to the second order event plane are shown in Fig. 2 and have been fitted to (3) to determine  $v'_{22}$ . For both orders, the fits have been made keeping terms up to values of  $n \cdot m = 2$  in the summation in (3).

The  $v'_{nm}$  are the values determined with respect to the estimated event plane and must be corrected for the event plane resolution [32] to obtain the actual anisotropy values

$$v_{nm} = \frac{\sqrt{2} \cdot v'_{nm}}{\text{RCF}_{nm}} \quad (8)$$

The factor  $\sqrt{2}$  arises because the particle distributions have been obtained with respect to the event plane of a subevent with half of the total event multiplicity. The subevent resolution,  $\sqrt{\langle \cos(nm(\psi_n'^a - \psi_n'^b)) \rangle}$ , is averaged over all events and is in good agreement with  $\text{RCF}_{nm}/\sqrt{2}$ .

In the third method, the values  $v_{nn}$  have been obtained directly by the subevent method from  $\chi_m$  of (5) and the fluctuation in the average multiplicity  $M$  of the full events in that centrality bin.

$$v_{nn} = \frac{\chi_n}{\sqrt{2M}} \quad (9)$$

The different methods yield consistent results for both the first order and the second order anisotropy coefficients and the difference in the values is included in the systematic error. The equivalence of the first two methods arises due to the equivalence of the geometric mean (method

1) and the arithmetic mean (method 2) of the resolution uncorrected values  $v'_n$  of the two subevents and due to the  $1/\sqrt{M}$  dependence of the fluctuation in event plane determination. The latter contributes to the equivalence of the third method with the first two. The three methods may yield different values in the presence of non-flow correlations where the differences will be governed by the nature and strength of these correlations. The most probable values are determined using method 1 above. The following sections discuss the systematic effects that distort the measured anisotropies and the centrality dependence of the anisotropies for charged particles and for photons.

## 4 Anisotropy in charged particles

The measured anisotropy is expected to be less than the actual anisotropy due to the finite granularity of the detector. The measured values of anisotropy may also be affected by the imprecision in the vertex position due to the finite spread of the beam. These effects are particularly relevant for the charged particle distribution measurement due to the relatively coarse segmentation and close proximity to the target of the SPMD detector. The effects are estimated using simulations.

### 4.1 Granularity

The finite granularity of the SPMD detector causes a dilution of the anisotropy of the azimuthal distribution primarily due to efficiency losses from multiple hits. The quantitative effect of the finite granularity on the measured anisotropy has been estimated and is briefly discussed in the following. This has been corroborated by simulations and is described in greater detail in [34].

Defining the mean occupancy as the ratio of the number of particles incident on the detector to the number of active cells

$$\mu = \frac{N_{\text{part}}}{N_{\text{cell}}} \quad (10)$$

one can show that

$$\mu = \ln \left( 1 + \frac{N_{\text{occ}}}{N_{\text{unocc}}} \right) \quad (11)$$

where  $N_{\text{occ}}$  and  $N_{\text{unocc}}$  are the number of occupied and unoccupied cells [35]. One can further show that

$$\frac{N_{\text{hit}}}{N_{\text{part}}} = \frac{1 - e^{-\mu}}{\mu} \quad (12)$$

where  $N_{\text{hit}}$  is the number of occupied cells.

Since the intrinsic occupancy of cells increases with the increase in the number of incident particles, the occupancy will have the same azimuthal dependence as the incident particles. Substituting this for the occupancy in (12) gives us the azimuthal dependence of the hits. Expressing the

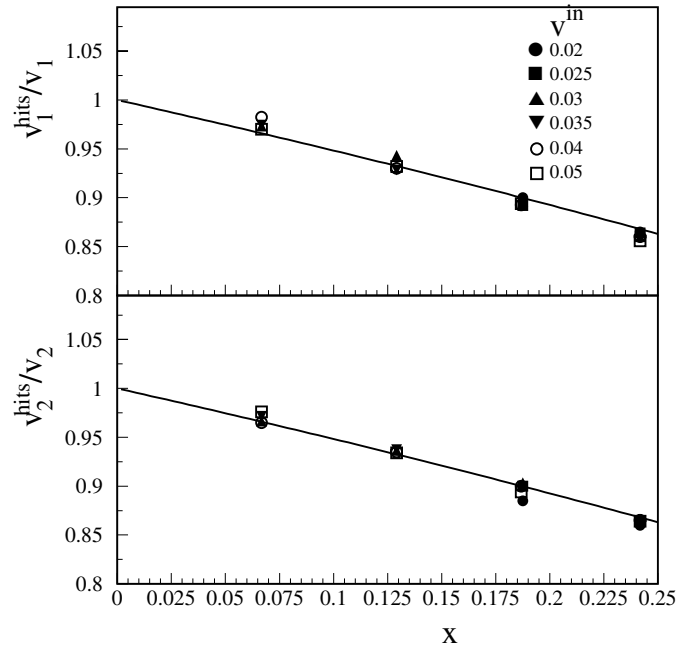


**Fig. 3.** The ratio  $v_n^{\text{hits}}/v_n$  for different number of occupied cells.  $x$  is the number of occupied cells scaled with the total number of cells. Different symbols correspond to different initial values of  $v_n$ . The solid line represents (13)

resulting equation as a Fourier series and collecting coefficients of  $\cos n\phi$  enables a determination of the ratio  $v_n^{\text{hits}}/v_n$ , which to first order can be approximated by

$$\frac{v_n^{\text{hits}}}{v_n} = -\frac{1-x}{x} \cdot \ln(1-x) \quad (13)$$

where  $x = \frac{N_{\text{hit}}}{N_{\text{cell}}} (= \frac{N_{\text{occ}}}{N_{\text{cell}}})$ .

The anisotropy in the distribution of charged particles can be obtained using the measured value of anisotropy in the distribution of hits.

The azimuthal distributions of the charged particles were generated with different initial anisotropies with multiplicities corresponding to the measured results. The charged particle hits were sorted into the SPMD bins ( $2^\circ$   $\phi$ -bin) assuming a 94% detection efficiency but taking into account hit losses due to multiple hits in a single SPMD pad. The resulting azimuthal distributions were then analyzed to determine the anisotropy coefficients using the method detailed in Sec 3.4 above. Figure 3 shows the results of the simulation for both orders, where the ratio of the estimated anisotropy from the hit distribution to the initial anisotropy is shown for varying hit multiplicities, far beyond the range of measured values in the SPMD. This is done for different values of initial anisotropy. The correction factor as given by (13) is shown as a solid line in the figure. One observes that the simulation results corroborate the results obtained above. The simulation results show that the extracted anisotropy is systematically lower than the initial anisotropy. Part of this loss occurs directly due to efficiency losses from multiple hits, and contributes both to the anisotropy and the event plane resolution.

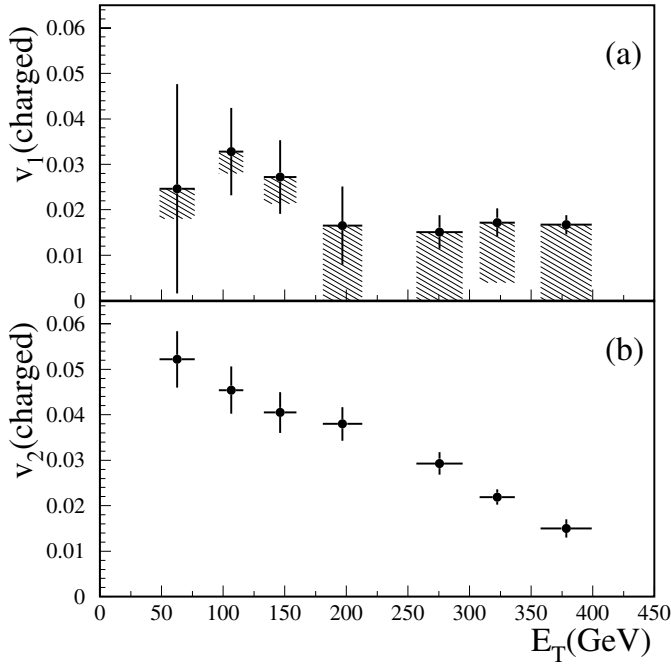


**Fig. 4.** Anisotropy coefficients of the azimuthal distributions of charged particles in the pseudorapidity region  $3.25 \leq \eta \leq 3.75$  for different centralities characterised by the measured transverse energy. **a** First order,  $v_1$ , where the shaded region indicates the extent of the total systematic error due to uncertainty in the vertex position. **b** Second order,  $v_2$

#### 4.2 Shift in vertex and beam spread

The finite beam size caused an imprecision in the assumed vertex by up to one mm in the WA98 experiment. A small shift in the vertex position does not affect the azimuthal distribution in the fine granularity PMD, situated at 21.5 meters from the vertex. However, it can produce an apparent anisotropy in the hit distribution in the SPMD situated at 0.328 meters from the target.

The effect of vertex shifts due to the beam spread was also investigated by simulation. The vertex position was generated according to a two dimensional Gaussian with width  $\sigma$ . Particles were simulated to originate from this vertex position with a realistic  $\eta$  and  $p_T$  distribution and an azimuthally symmetric  $\phi$  distribution. The particles were projected onto the SPMD plane, and their hit positions recorded according to the granularity and nominal location of the SPMD detector. The recorded positions corresponded to values of  $\eta$  and  $\phi$  which differed from the generated values due to the shifted position of the vertex. The simulated distributions were then analyzed in the same manner as the experimental data. This was repeated for different values of  $\sigma$  and the values of  $v_n$  were obtained for each sample generated. The maximum possible shift has been deduced by assuming an azimuthally symmetric distribution for the most central class, and assigning the granularity corrected observed value for first order anisotropy to the shift in vertex. This corresponded to a maximum width of the Gaussian distribution due to beam spread of 0.3 mm.

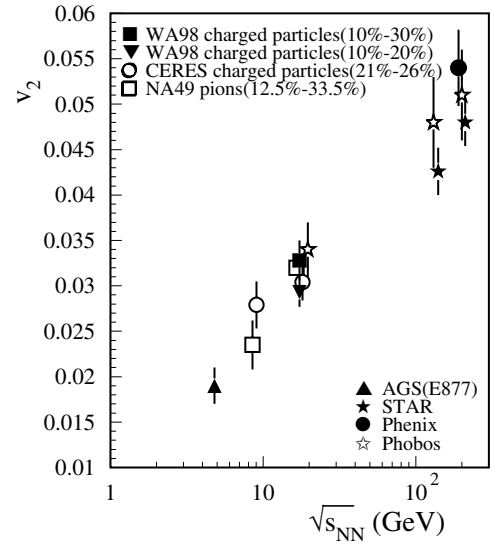


**Fig. 5.** Second order coefficient for different centre of mass energies. The results of the present work are for charged particles and are shown for two different centrality classes. The ordinates of CERES, NA49, STAR and PHENIX results have been shifted slightly for clarity. The error bars on WA98 points indicate the statistical and systematic errors added in quadrature. E877, STAR, PHENIX and PHOBOS  $v_2$  values are for charged particles. The centrality cuts for all experiments are comparable

A shift in the vertex position due to beam spread, or time variation during the 2.5 s SPS spill, produces an azimuthal distribution which has a shifted centroid. If the shift occurs on an event-by-event basis it cannot be corrected for by the acceptance correction methods discussed above, since they can only correct for average effects. To investigate the possibility of systematic shifts correlated with time during the SPS spill, the SPMD charged particle azimuthal distributions were analyzed for different times during the spill. No significant variations with time during the spill were observed.

The second order anisotropy is obtained from the fit to the elliptical shape of the measured hit distribution. A vertex shift does not affect the elliptical shape, as verified by simulations.

#### 4.3 Results

The finite granularity requires a correction which is obtained using the measured values of  $v_n$  from the hit distributions and using (13). The corrected results are shown for both orders of anisotropy in Fig. 4. The error bars shown are statistical. The results for the first order anisotropy include contributions from a possible vertex shift. The upper and the lower limit of the boxes shown in Fig 4a show the asymmetric systematic error and correspond to no uncertainty and a maximum uncertainty in the position of the vertex, as discussed above.

Figure 5 shows  $v_2$  as a function of centre of mass energy from various experiments (results mostly taken from com-



pilation of [36]). These have been measured in different experiments in different kinematic ranges using methods that vary in detail. The general behaviour shows a continuous increase in  $v_2$  as a function of centre of mass energy. The results of the present work are shown for two different centrality ranges corresponding to 10–20% of cross section and 10–30% of cross section. For comparison to the present results, values of  $v_2$  from PHOBOS, NA49 and CERES experiments [35–37] at nearly the same centre of mass energy are included. The various measurements are seen to agree well within errors.

## 5 Anisotropy in photons

The photons incident on the PMD predominantly result from the two photon decay of the neutral pion, and if both photons are detected in the PMD an additional apparent anisotropy will result from the kinematic correlation between the photons. The limited efficiency and purity of the detected photon sample in the PMD affect the measured photon anisotropy values. The quantitative effect is estimated using simulations and is described in the following.

### 5.1 Decay effect

The decay of neutral pions into two photons introduces correlations that can cause apparent anisotropies in the photon distributions which are greater than the actual anisotropy of the pions. On the other hand, the process of decay smears the photon momenta relative to the initial pion momenta and can thereby dilute the initial correlation present in the neutral pions. The relative importance of these two competing effects has been shown to scale with the experimentally measured quantity  $\chi_m$  and enables a determination of the neutral pion anisotropy from the measured photon anisotropy [23]. However, the limited efficiency and the contamination of charged particles in the sample preclude a determination of the  $\pi^0$  anisotropy from the measured  $\gamma$  anisotropy in the present work. Using the anisotropy values of the charged particles folded with the  $\pi^0$  decay and experimental response allows one to determine the expected values of anisotropy of the photons in the PMD, as discussed below.

### 5.2 Efficiency and contamination

The PMD records particle hits which include incident photons and a contamination of charged particle hits. These charged particles could be primary, or secondary rescattered particles. As noted above, the photon counting efficiency ( $\epsilon$ ) of the sample varies from 68% to 73% for central and peripheral events and the corresponding purity ( $p$ ) of the sample varies from 65% to 54%.

The effect of decay, identification efficiency, and contamination on the observed photon anisotropy has been estimated using simulations. The simulations assume that the photon sample contains a contribution from charged

**Table 2.** Contribution to systematic error from various sources for the simulated values of both orders of anisotropy of the  $N_{\text{photons}}$  distributions for the centrality selection corresponding to 20–30% of minimum bias cross section

Source	First order	Second order
	+0.005	+0.002
Charged particle anisotropy	−0.004	−0.003
Purity of photon sample	$\pm 0.002$	$\pm 0.001$
Anisotropy of contaminants	−0.004	−0.007
$\eta$ and $p_T$ distribution of $\pi^0$	$\pm 0.001$	$\pm 0.001$
Neutral pion multiplicity	$\pm 0.002$	$\pm 0.001$

particle contamination which directly reflects the measured charged particle anisotropy in addition to a contribution from photons from  $\pi^0$  decays with a  $\pi^0$  anisotropy which is also equal to the measured charged particle anisotropy. These simulations use the anisotropy values of the charged particles,  $\pi^0$  decay kinematics, the PMD acceptance, and the purity of the PMD photon sample to generate simulated data. The simulated sample is analyzed to obtain an estimate of the expected photon anisotropy corresponding to the observed charged particle anisotropy.

The neutral pions were generated using the experimental pseudorapidity distribution of the charged pions [38] with an exponential  $p_T$  distribution ( $dN/dp_T = p_T \cdot \exp(-6p_T)$ ). The  $\pi^0$  multiplicity values were chosen as half of those measured for charged particles with the SPMD for the same centrality selection. The second order anisotropy values of  $\pi^0$  were chosen to be linearly increasing with  $p_T$  before saturating at  $p_T \sim 1.5$  GeV/c. For each centrality, the  $p_T$  dependence was chosen to reproduce the  $p_T$  integrated mean values of  $v_n$  of charged particles shown in Fig. 4. The linear dependence and the value of  $p_T$  at saturation were both varied to estimate the systematic errors. Neutral pions were generated and decayed and the decay photons were accepted if within the PMD acceptance. Using the measured photon multiplicity for a given centrality class,  $p \cdot N_{\text{photons}}$  photons were randomly selected from those falling onto the PMD, where  $p$  was assigned a value of 0.65 to 0.54 corresponding to the centrality selection being simulated. A background contribution of  $(1 - p) \cdot N_{\text{photons}}$  charged particles was added to the simulated event. This simulated data was then analyzed using the methods detailed in Sect. 3.4.

The systematic errors in the simulated results have been estimated for both orders of anisotropy for each centrality. The contribution to the systematic error on the simulated results are shown for one particular centrality selection (20%–30% of minimum bias cross section) in Table 2.

The relation between the neutral pion anisotropy and photon anisotropy is not linear [23].  $v_n^{\text{PMD}}$  has been estimated for a range of pion anisotropy values corresponding to the error measured in this experiment. An increase

(decrease) in the charged particle anisotropy increases (decreases) the anisotropy in the simulated results of  $v_n^{\text{PMD}}$  for all centralities. The percentage change in  $v_n^{\text{PMD}}$  corresponding to a 10% change in the purity of photon sample is small and is about the same for all centralities. If 50% of the contaminants are assumed to be isotropic, then the resulting anisotropy decreases for all centralities, and contributes maximally to the total systematic error. The uncertainty in the neutral pion multiplicity also has a small effect, which is almost independent of centrality.

The systematic error on the measured values of  $v_n^{\text{PMD}}$  have been obtained by

- increasing and decreasing the region of acceptance for the analysis
- varying the size of the interval  $\Delta\eta$  between the two subevents in the range 0.03 to 0.07.
- randomly removing up to 20% of the photons in the PMD.
- obtaining the  $v_n^{\text{PMD}}$  values by the correlation between the subevents as described in Sect. 3.4 above.

Repeating the analysis by rejecting clusters closer than twice the size of the scintillator pads did not change the  $v_n^{\text{PMD}}$  values.

### 5.3 Results

The measured values of  $v_n^{\text{PMD}}$  are shown in Fig. 6. The errors on  $v_n^{\text{PMD}}$  are obtained by adding the systematic and the statistical error in quadrature and are also shown. The open triangles show the expected values of  $v_n^{\text{PMD}}$  from the simulations described above. The statistical and systematic errors are added in quadrature and are shown by the shaded regions. The photon anisotropy coefficients extracted from the simulated PMD data are consistent within errors with the measured PMD result. This demonstrates that the photon anisotropy results measured with the PMD are consistent with the charged particle results presented in Sect. 4. Note, however, that the results shown in Fig. 6 include  $\pi^0$  decay and charged particle contamination effects, and should not be compared directly with other results. In particular, the use of the PMD photons themselves to determine the event plane gives a strong  $\pi^0$  decay effect. This is shown by the open circles in Fig. 6 which show the simulation values of  $v_n^{\text{PMD}}$  for the assumption of isotropic  $\pi^0$  emission,  $v_n(\pi) = 0$ . It is seen that the first order photon anisotropy results are dominated by the  $\pi^0$  decay effect while the second order photon anisotropy results also have a significant decay contribution, which cannot simply be subtracted from the measured  $v_2^{\text{PMD}}$ . Since the relationship between  $v_\gamma$  and  $v_{\pi^0}$  depends in a non-trivial way on the  $\pi^0$  ( $p_T$  dependent) multiplicity and anisotropy [23, 39] it is non-trivial to extract the  $\pi^0$  anisotropy from the photon anisotropy measured with respect to the event plane determined using photons. It should be noted that the WA98 photon  $v_n$  results measured with the LEDA photon detector covering the photon rapidity region  $2.3 \leq y \leq 2.9$  [39] were obtained with respect to an event plane determined in the target fragmentation region. The  $v_n^{\text{PMD}}$  measured using the PMD photons and

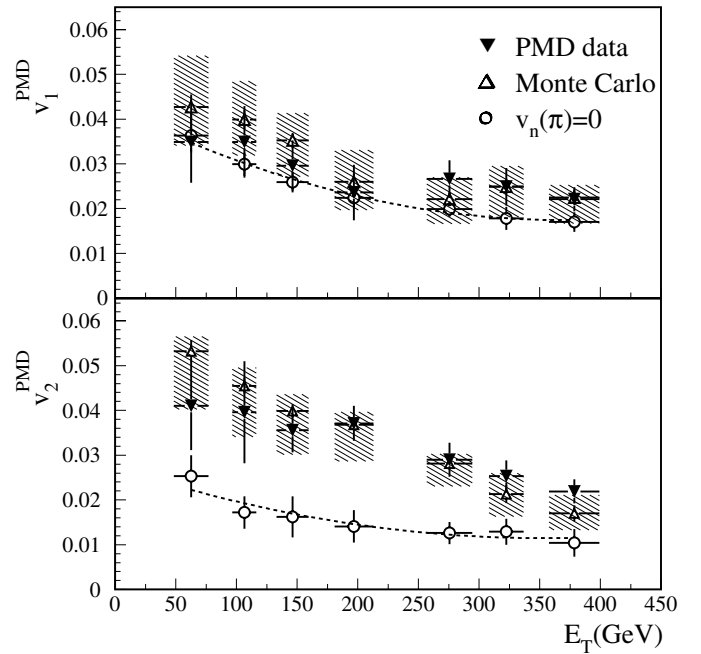


**Fig. 6.** **a** First order,  $v_1^{\text{PMD}}$ , and **b** second order,  $v_2^{\text{PMD}}$ , photon anisotropy coefficients in the pseudorapidity region  $3.25 \leq \eta \leq 3.75$  for different centralities are shown by filled triangles. Statistical and systematical errors are added in quadrature and shown as bars on the filled triangles. Open triangles are the most probable values of  $v_n^{\text{PMD}}$  as expected from the simulation. The shaded regions indicate the simulation uncertainties as described in Sect. 5.4. The open circles show the calculated values of  $v_n^{\text{PMD}}(v_n(\pi) = 0)$  assuming an isotropic distribution of pions with the dashed curve indicating a smooth polynomial fit to the open points. Note, however, that  $v_n^{\text{PMD}}(v_n(\pi) = 0)$  can not be directly subtracted from the  $v_n^{\text{PMD}}(v_n(\pi) > 0)$  to obtain the anisotropy flow coefficients  $v_n$ , as explained in the text

$v_n$  measured using the LEDA photons will therefore have different sensitivity to the  $\pi^0$  decay effect. The PMD results include effect of decay correlations, and therefore the current measurement,  $v_n^{\text{PMD}}$ , provides upper limits on the anisotropic flow coefficients  $v_n$ .

## 6 Summary

The azimuthal angle distributions with respect to the event plane have been measured for charged particles and photons with full azimuthal coverage in the pseudorapidity region of  $3.25 \leq \eta \leq 3.75$  for  $^{208}\text{Pb} + ^{208}\text{Pb}$  collisions at  $158 \cdot A \text{ GeV}/c$ . A total of 0.25 million events, classified in seven centrality selections, have been used in the analysis. The Fourier coefficients of the azimuthal distributions have been extracted in several ways, all giving consistent results for the first order  $v_1$  (directed) and  $v_2$  second order (elliptic) anisotropies for photons and charged particles. The results show the expected trend of decreasing anisotropy with increasing centrality for both  $v_1$  and  $v_2$  for charged particles and photons. Our results agree with the

results reported by other experiments for near similar conditions. [35–37,39]. The observed anisotropies of the photon distributions compare well with those obtained from simulations that include the charged particle contamination and the correlations arising due to the decay of the neutral pions assumed to have the same anisotropies as measured for charged particles.

*Acknowledgements.* We wish to express our gratitude to the CERN accelerator division for the excellent performance of the SPS accelerator complex. We acknowledge with appreciation the effort of all engineers, technicians, and support staff who have participated in the construction of this experiment.

This work was supported jointly by the German BMBF and DFG, the U.S. DOE, the Swedish NFR and FRN, the Dutch Stichting FOM, the Polish KBN under Contract No. 621/E-78/SPUB-M/CERN/P-03/DZ211/, the Grant Agency of the Czech Republic under contract No. 202/95/0217, the Department of Atomic Energy, the Department of Science and Technology, the Council of Scientific and Industrial Research and the University Grants Commission of the Government of India, the Indo-FRG Exchange Program, the PPE division of CERN, the Swiss National Fund, the INTAS under Contract INTAS-97-0158, ORISE, Grant-in-Aid for Scientific Research (Specially Promoted Research & International Scientific Research) of the Ministry of Education, Science and Culture, the University of Tsukuba Special Research Projects, and the JSPS Research Fellowships for Young Scientists. ORNL is managed by UT-Battelle, LLC, for the U.S. Department of Energy under contract DE-AC05-00OR22725. The MIT group has been supported by the US Dept. of Energy under the cooperative agreement DE-FC02-94ER40818.

## References

1. H.A. Gustafsson et al., Phys. Rev. Lett. **52**, 1590 (1984); H.H. Gutbrod et al., Phys. Lett. B **216**, 267 (1989); H.H. Gutbrod et al., Rep. Prog. Phys. **52**, 1267 (1989); H.H. Gutbrod et al., Phys. Rev. C **42**, 640 (1990)
2. W. Reisdorf, H.G. Ritter, Ann. Rev. Nucl. Part. Sci. **47**, 663 (1997)
3. EOS Collaboration, J. Chance et al., Phys. Rev. Lett. **78**, 2535 (1997); M.A.Lisa et al., nucl-ex/9610007
4. FOPI Collaboration, G. Poggi et al., Nucl. Phys. A **586**, 755 (1995); J.L. Ritman et al., Z. Phys. **352**, 355 (1995); N. Bastid et al., Nucl. Phys. A **622**, 573 (1997)
5. KaoS Collaboration, D. Bril et al., Phys. Rev. Lett. **71**, 336 (1993); D. Brill et al., Z. Phys. A **355**, 61 (1996); Y. Shin et al., Phys. Rev. Lett. **81**, 1576 (1998)
6. E877 Collaboration, J. Barette et al., Phys. Rev. Lett. **73**, 2532 (1994); Phys. Rev. Lett. **70**, 2996 (1993); Phys. Rev. C **55**, 1420 (1997); Phys. Rev. C **56**, 3254 (1997)
7. E802 Collaboration, L. Ahle et al., Phys. Rev. C **57**, 1416 (1998)
8. WA93 Collaboration, M.M. Aggarwal et al., Phys. Lett. B **403**, 390 (1997)
9. WA98 Collaboration, M.M. Aggarwal et al., Phys. Lett. B **469**, 30 (1999)
10. NA49 Collaboration, T. Wienold et al., Nucl. Phys. A **610**, 76c (1996); H. Appelshäuser et al., Phys. Rev. Lett. **80**, 4136 (1998)
11. STAR Collaboration, K.H. Ackermann et al., Phys. Rev. Lett. **86**, 402 (2001); C. Adler et al., Phys. Rev. Lett. **87**, 182301 (2001)
12. PHENIX Collaboration, K. Adcox et al., Phys. Rev. Lett. **89**, 212301 (2002); S. Esumi et al., Nucl. Phys. A **715**, 599c (2003)
13. PHOBOS Collaboration, B.B. Back et al., Phys. Rev. Lett. **89**, 222301 (2002)
14. P. Danielewicz et al., Phys. Rev. Lett. **81**, 2438 (1998); Nucl. Phys. A **661**, 82c (1999)
15. G.Q. Li, C.M. Ko, B. Li, Phys. Rev. Lett. **74**, 235 (1995); H. Sorge, Phys. Rev. C **52**, 3291 (1995)
16. H. Heiselberg, Anne-Marie Levy, Phys. Rev. C **59**, 2716 (1999)
17. J.-Y. Ollitrault, Phys. Rev. D **46**, 229 (1992)
18. P.F. Kolb et al., Nucl. Phys. A **696**, 197 (2001)
19. P.F. Kolb, J. Sollfrank, U.W. Heinz, Phys. Rev. C **62**, 054909 (2000)
20. H. Sorge, Phys. Rev. Lett. **78**, 2309 (1997)
21. H. Sorge, Phys. Rev. Lett. **82**, 2048 (1999)
22. S.A. Voloshin, A.M. Poskanzer, Phys. Lett. B **474**, 27 (2000)
23. R. Raniwala, S. Raniwala, Y.P. Viyogi, Phys. Lett. B **489**, 9 (2000)
24. Gobinda Mishra, Ph.D thesis, Utkal University, 1999
25. Sudhir Raniwala, Pramana-Journal of Physics **60**, 739 (2003)
26. Proposal for a Large Acceptance Hadron and Photon Spectrometer, Preprint CERN/SPSLC 91-17, SP-SLC/P260
27. WA98 Collaboration, M.M. Aggarwal et al., Phys. Lett. B **420**, 169 (1998)
28. W.T. Lin et al., Nucl. Instrum. Meth. A **389**, 415 (1997)
29. M.M. Aggarwal et al., Nucl. Instrum. Methods Phys. Res. A **424**, 395 (1999)
30. WA98 Collaboration, M.M. Aggarwal et al., Phys. Lett. B **458**, 422 (1999)
31. T. C. Awes et al., Nucl. Instrum. Methods Phys. Res. Sect. A **279**, 497 (1989)
32. A.M. Poskanzer, S. Voloshin, Phys. Rev. C **58**, 1671 (1998)
33. J.-Y. Ollitrault, e-print nucl-ex/9711003
34. R. Raniwala, S. Raniwala, Y.P. Viyogi, e-print nucl-ex/0502023
35. PHOBOS Collaboration, B.B. Back et al., nucl-ex/0406021
36. NA49 Collaboration, C. Alt et al., Phys. Rev. C **68**, 034903 (2003)
37. CERES/NA45 Collaboration, J. Slivova et al., Nucl. Phys. A **715**, 615c (2003)
38. WA98 Collaboration, M.M. Aggarwal et al., Eur. Phys. J. C **18**, 651 (2001)
39. WA98 Collaboration, M.M. Aggarwal et al., nucl-ex/0410045